Supplemental Information

Low hydrogen crossover anion-exchange membrane water electrolysis based on non-ionic binder polymers

Oscar Strobl[1*], Nemanja Martic[1*], Hannes Michaels[1*], Felipe Not de Godoy[1], Franka Wessnick[1], Daniel Lang[1], Michael Kress[1], Anna Maltenberger[1], Sönke Wengler-Rust[2], Thomas Luxbacher[3], Steffen Falgner[2], Patrick Borowski[4], Artjom Maljusch[4], Andre Klinger[1], Günter Schmid[1]

[1] Siemens Energy Global GmbH and Co. KG, Schuckertstrasse 2, 91058 Erlangen, Germany
[2] Anton Paar Germany GmbH, Hellmuth-Hirth-Strasse 6, 73760 Ostfildern-Scharnhausen, Germany
[3] Anton Paar GmbH, Anton-Paar-Strasse 20, 8054 Graz, Austria
[4] Evonik Operations GmbH, Research, Development & Innovation, Paul-Baumann-Straße 1, 45772 Marl, Germany

*These authors contributed equally.
[†] Correspondence: hannes.michaels@siemens-energy.com

Contents

Electrochemical testing setup.

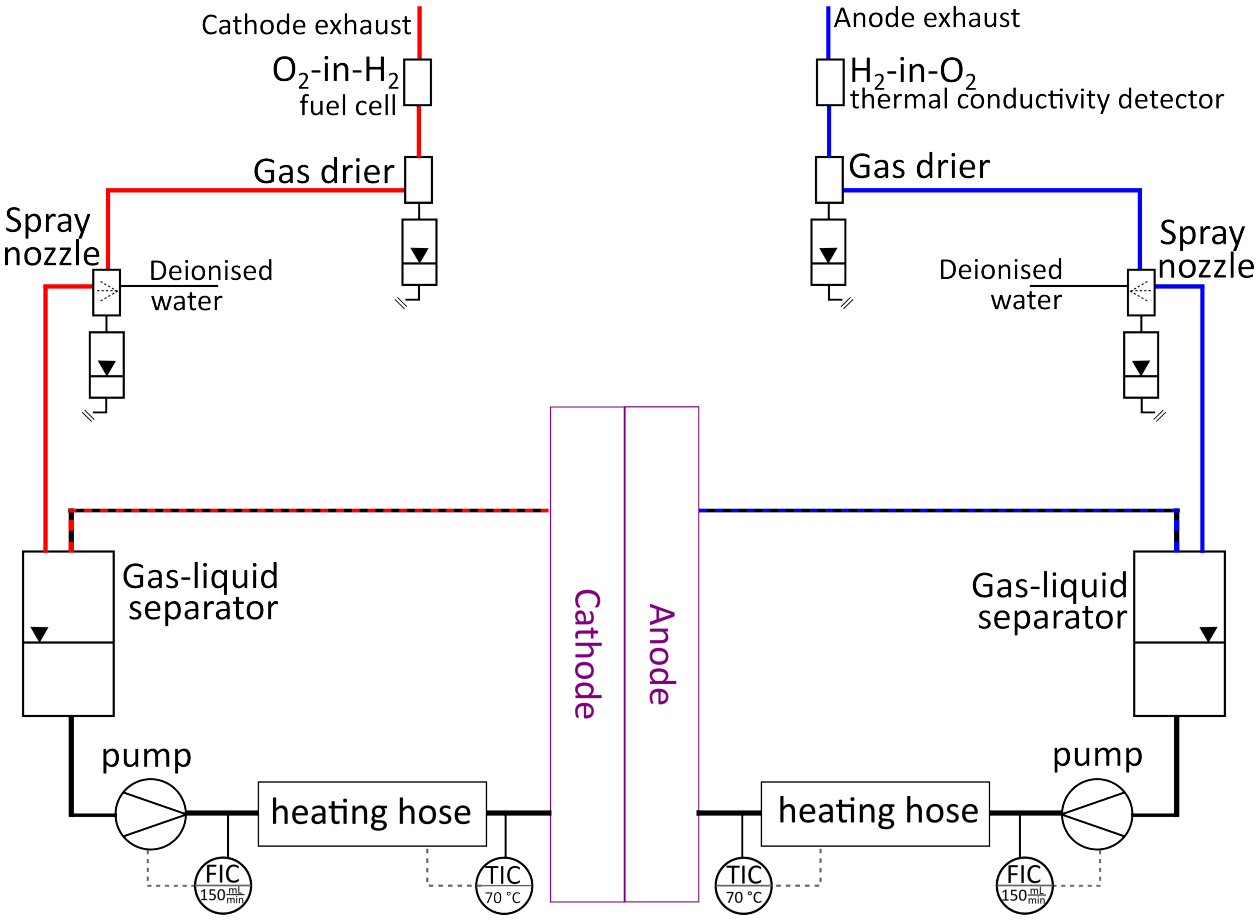

Figure S1: Setup for electrochemical testing.

Flux model derivation

The mathematical model to describe the flux of hydrogen was adapted from earlier efforts from our group.[S1] The reader is referred to the earlier publication for a detailed derivation of the solubility and permeability of hydrogen gas in potassium hydroxide solutions as functions of temperature and lye concentration. Hereinafter, values for hydrogen in the employed 1 M KOH electrolyte at 70 °C are used, namely a solubility $S^{\mathrm{elec}}_{\mathrm{H_2}}$ of 5.2 10^{-6} mol m^{-3} Pa^{-1} a diffusion coefficient $D^{\mathrm{elec}}_{\mathrm{H_2}}$ of 9.1 10^{-9} m^2 s^{-1} and a permeability $P^{\mathrm{elec}}_{\mathrm{H_2}}$ of 4.7 10^{-14} mol m^{-2} s^{-1} Pa^{-1}.
The following derivation assumes an even distribution of current across the 25 cm^2 active area and negligible effects of e.g. parasitic OH^- ionic currents. It further examines the fluxes of gases and liquids solely in z-direction (i.e., through the membrane), and neglects any gradients in x, y-directions. The amount of hydrogen gas generated through the electrolysis reaction $\sigma_{\mathrm{H_2}}$ (in

mol $m^{-2}s^{-1}$) is proportional to the applied geometric current density j_{geo}

$$\sigma_{\mathrm{H_2}} = \frac{j_{\mathrm{geo}}}{2F} \tag{S1}$$

where F is Faraday's constant, assuming unity faradaic efficiency towards hydrogen evolution at the cathode.

In the assumption of a thin reaction front (i.e., the majority of hydrogen gas evolving in a thin region of the catalyst layer closest to the membrane), we assume the simplification that the hydrogen gas evolves at a balance plane between the cathode and the membrane. The sum of any of transport processes $J^i_{\mathrm{H_2}}$ (in mol $m^{-2}s^{-1}$) comprising hydrogen gas must therefore, in a constant-current-hold, add up to the source term. Transport processes in this derivation include transport of hydrogen gas into the cathode bulk ($J^{\mathrm{bulk}}_{\mathrm{H_2}}$), as well as hydrogen crossover processes caused by diffusion ($J^{\mathrm{diff}}_{\mathrm{H_2}}$) and electroosmotic drag ($J^{\mathrm{drag}}_{\mathrm{H_2}}$). All expressions assume steady-state operation under constant current. It is noted here that transport processes in either physical direction (i.e., through the membrane or towards the cathode bulk) account similarly towards the distribution away from this single balance plane.

$$\sigma_{\mathrm{H_2}} = \sum_i^n J^i_{\mathrm{H_2}} = J^{\mathrm{bulk}}_{\mathrm{H_2}} + J^{\mathrm{diff}}_{\mathrm{H_2}} + J^{\mathrm{drag}}_{\mathrm{H_2}} \tag{S2}$$

Hydrogen transport out of the cathode.

The evolution of hydrogen gives rise to an elevated concentration of dissolved hydrogen gas at the balance plane $c^*_{\mathrm{H_2}}$. In the desired case, the produced hydrogen is transported away from the balance plane, through the catalyst layer towards the bulk electrolyte ($J^{\mathrm{bulk}}_{\mathrm{H_2}}$). The driving force for this process is the difference in dissolved hydrogen concentration from the balance plane $c^*_{\mathrm{H_2}}$ to the bulk cathode electrolyte $c^c_{\mathrm{H_2}}$. As the rate constant for this process, a mass transport velocity k_l (in m s^{-1}) is introduced.

Using Henry's law $c_i = S_i \cdot p_i$, the gas pressures $p^*_{\mathrm{H_2}}$ and $p^{\mathrm{c}}_{\mathrm{H_2}}$ are obtained from the dissolved gas concentrations $c^*_{\mathrm{H_2}}$ and $c^{\mathrm{c}}_{\mathrm{H_2}}$ and the solubility of hydrogen in the electrolyte $S^{elec}_{H_2}$. During a constant-current-hold of the electrolyser, it is assumed that O_2 in H_2 gas impurities are low and therefore in the bulk electrolyte, $p^c_{\mathrm{H_2}}$ = p^{c} and the effective operating pressure of 1.15 bar is assumed.

$$J^{\mathrm{bulk}}_{\mathrm{H_2}} = k_l \left(c^*_{\mathrm{H_2}} - c^c_{\mathrm{H_2}}\right) = k_l S^{\mathrm{elec}}_{\mathrm{H_2}} \left(p^*_{\mathrm{H_2}} - p^c_{\mathrm{H_2}}\right) \tag{S3}$$

Hydrogen crossover by Diffusion.

Simultaneously, undesired hydrogen crossover can occur, driven this time by the difference in dissolved hydrogen concentration from the balance plane $c^*_{\mathrm{H_2}}$ to the bulk concentration in the anode electrolyte $c^a_{\mathrm{H_2}}$

$$J^{\mathrm{diff}}_{\mathrm{H_2}} = \frac{D^{\mathrm{eff}}_{\mathrm{H_2}}}{\delta_{\mathrm{m}}} \left(c^*_{\mathrm{H_2}} - c^{\mathrm{a}}_{\mathrm{H_2}}\right) \tag{S4}$$

where $D^{\mathrm{eff}}_{\mathrm{H_2}}$ is the effective diffusion coefficient of hydrogen gas through the KOH-swollen membrane and δ_{m} the membrane thickness. During a constant-current-hold, it is assumed that the anode is filled with O_2 gas, and therefore $c^{\mathrm{a}}_{\mathrm{H_2}} = S^{\mathrm{elec}}_{\mathrm{H_2}} p^{\mathrm{a}}_{\mathrm{H_2}} \approx 0$ mol L^{-1} and $J^{\mathrm{diff}}_{\mathrm{H_2}} = \frac{D^{\mathrm{eff}}_{\mathrm{H_2}}}{\delta_{\mathrm{m}}} c^{*}_{\mathrm{H_2}}$.

Electroosmotic drag.
OH^- ions move across the AEM from cathode to anode along the electric field. The hydroxide ions are hydrated by water molecules, which are in turn dragged along across the membrane. In membrane electrolysis technologies, it has therefore been established to define a drag coefficient ξ, specifying how many water molecules are pulled along with each transported ion.

$$J^{\mathrm{drag}}_{\mathrm{H_2O}} = \frac{j_{\mathrm{geo}}}{F} \xi \tag{S5}$$

This number has been reported to depend on e.g. the membrane type (e.g. PEM *vs* AEM), the polymer chemistry, as well as current density and salt concentration in the liquid electrolyte.[S2] The drag coefficient is obtained experimentally by reading the temporal evolution of the anode and cathode fill levels in the electrolyte tanks at any given (constant) current density (see Fig. S6). For the here evaluated Evonik membrane system and conditions, the drag coefficient is estimated around 1.5 H_2O per OH^-, essentially independent of current density (see Fig. S7).
This hydration shell around the hydroxide ions may contain dissolved hydrogen gas. By these means, hydrogen may be transferred from the cathode to the anode electrolyte, contributing to the hydrogen crossover. The concentration of dissolved hydrogen gas (per unit volume of liquid electrolyte) at the boundary layer was described above as $c^{*}_{\mathrm{H_2}}$. The effective concentration of water molecules per unit volume of liquid electrolyte $c^{\mathrm{elec}}_{\mathrm{H_2O}}$ was derived concentration- and temperature-dependent in our previous report.[S1] The here-described conditions of 1 M KOH at 70 °C give 52 mol L^{-1}. The ratio of the two concentrations therefore gives the count of dissolved hydrogen molecules per water molecule.

$$J^{\mathrm{drag}}_{\mathrm{H_2}} = \frac{j_{\mathrm{geo}}}{F} \xi \frac{c^{*}_{\mathrm{H_2}}}{c^{\mathrm{elec}}_{\mathrm{H_2O}}} = \frac{j_{\mathrm{geo}}}{F} \xi \frac{S^{\mathrm{elec}}_{\mathrm{H_2}} p^{*}_{\mathrm{H_2}}}{c^{\mathrm{elec}}_{\mathrm{H_2O}}} \tag{S6}$$

Supersaturation pressure and mass balance
The generation term from Eq. (S1) and the individual distribution fluxes from Eqs. (S3)-(S6) are entered into Eq.(S2). The obtained mass balance is solved for the supersaturation pressure at the balance plane $p^{*}_{\mathrm{H_2}}$.

$$p^{*}_{\mathrm{H_2}} = \frac{\frac{j_{\mathrm{geo}}}{2F} + k_l S^{\mathrm{elec}}_{\mathrm{H_2}} p^{\mathrm{c}}_{\mathrm{H_2}}}{\frac{D^{\mathrm{eff}}_{\mathrm{H_2}} S^{\mathrm{elec}}_{\mathrm{H_2}}}{\delta_{\mathrm{m}}} + k_l S^{\mathrm{elec}}_{\mathrm{H_2}} + \frac{j_{\mathrm{geo}} \xi S^{\mathrm{elec}}_{\mathrm{H_2}}}{F c^{\mathrm{elec}}_{\mathrm{H_2O}}}}} \tag{S7}$$

with all denominator terms in [mol m^{-2}s^{-1}Pa^{-1}]. The experimentally measured hydrogen in the anode gas stream J_{exp} (in mol m^{-2}s^{-1}) is converted from the sensor reading $Y_{\mathrm{H_2}}$ (with dimensionless $0 \leqslant Y_{\mathrm{H_2}} \leqslant 1$). It is equal to the sum of both crossover flux contributions of diffusion and

electroosmotic drag. Note the $4F$ rather than $2F$ as Y_{H_2} represents a volume share in the oxygen stream.

$$J_{\mathrm{exp}} = \frac{Y_{\mathrm{H_2}}}{1 - Y_{\mathrm{H_2}}} \frac{j_{\mathrm{geo}}}{4F} = J_{\mathrm{H_2}}^{\mathrm{diff}} + J_{\mathrm{H_2}}^{\mathrm{drag}} \tag{S8}$$

To solve the mass balance, Eqs. (S4), (S6), (S7) and (S8) are leaving the two variables k_l and $D_{\mathrm{H_2}}^{\mathrm{eff}}$. The set of equations is solved for each set of $j_{\mathrm{geo}}, J_{\mathrm{exp}}(j_{\mathrm{geo}})$ data.

The authors note here that the above-described model is derived based on a number of much-simplified assumptions, such as a single balance plane of hydrogen generation and a current-density-independent transport mechanism (and therefore transport coefficient/velocity) of hydrogen out of the cathode catalyst layer. Nonetheless, the authors contend that the presented description adequately emphasises the effects of the electrode materials into key parameters regarding hydrogen crossover.

Contact angle and supersaturation pressure.

The exact description of the transport of gases and water through porous, partly-wetted electrodes in e.g. electrolyser and fuel cell electrodes has been described in great detail elsewhere.[S3,S4] In particular, pore wetting of electrode layers requires sophisticated descriptions: In most practical cases, electrolyser and fuel cell electrodes consist of broad pore size distributions, where large pores wet at lower pressures than smaller pores. The reader interested in mathematical modeling is therefore referred to the detailed literature above.

In the most fundamental approach, the capillary pressure $p_{\mathrm{H_2}}^{\mathrm{cap}}$ is the pressure difference between the gas and liquid phases:

$$p_{\mathrm{H_2}}^{\mathrm{cap}} = p_{\mathrm{H_2}}^{\mathrm{g}} - p_{\mathrm{H_2}}^{\mathrm{l}} \tag{S9}$$

For a cylindrical pore with the contact angle θ, the Young-Laplace capillary equation calculates the pressure required for gas to enter into liquid-filled pores.[S5,S6]

$$r(p, \theta) = \frac{2\gamma \cos\theta}{p_{\mathrm{H_2}}^{\mathrm{cap}}} \tag{S10}$$

where r is the pore radius, γ is the surface tension of the liquid (for 1 M KOH under the conditions of the presented experiments around 70.2 mN m^{-1})[S7], θ is the contact angle of the liquid on the specified surface, and $p_{\mathrm{H_2}}^{\mathrm{cap}}$ is the required capillary pressure. This allows the estimation of a *critical pore radius* r_{c}, where the gas pressure is able to de-wet pores. For the ionomer-based electrode with contact angle 68° at the highest supersaturation of 7 bar, a critical pore size of ≈75 nm is obtained. We find this consistent with other reports where catalyst layer average pore sizes were equally determined around 75 nm by means of FIB-SEM tomography[S8]; further, other literature usually reports the "secondary pore regime" which governs transport limit phenomena around some hundred nanometers.[S9,S10]

Nonetheless, this description does not yet explain the decreased pressure drop across three-dimensional electrode layers, especially in the case of the non-ionic electrodes with contact angles of 130°, as $\cos\theta$ drops below zero and the pore would not be stably liquid-filled under equilibrium conditions and intrinsically expel water against the external hydraulic pressure of the electrolyte.

In this case, capillarity does not oppose gas invasion but instead favors spontaneous de-wetting of sufficiently connected pores.
Further derivation of detailed physical parameters for the presented catalyst layers bears inherent uncertainties, as e.g. the effective contact angle inside pores of the electrode may differ from the bulk electrode contact angle depending on e.g. the local material composition[S11] and the specific pore size. Nonetheless, consider the start-up of an electrolyser. Before the application of electric current, the majority of pores is initially filled with electrolyte. Subsequently, gas evolution leads to hydrogen gas pushing the liquid out of those pores, whose radius is larger than r_c. Therefore, the share of secondary pores (≈50–300 nm) that remains filled with liquid $s_\mathrm{L}(\Delta p, \theta)$, defined as the fraction of pore volume occupied by electrolyte, comprises all pores smaller than r_c

$$s_\mathrm{L}(\Delta p, \theta) = \int_0^{r_c(\Delta p, \theta)} f(r)\,\mathrm{d}r \tag{S11}$$

where $f(r)$ denotes the (normalised) pore size distribution of the electrode. While the above derivation contains many unknown parameters, a first set of conclusions can be drawn from this description based on model assumptions for the purpose of practical visualisation of the presented phenomena. The porosity distribution of the prepared CCM-type electrodes is captured with high resolution down to the $<$ 1nm range by the here employed gas adsorption techniques. However, the techniques approach their limits towards $\gtrsim$50 nm. Therefore, for the purpose of elucidating how the contact angle influences further macroscopic electrode parameters, we here assume a hypothetical typical bimodal catalyst layer pore size distribution (2-20 nm, 50-300 nm)[S9,S10]. This allows the estimnation of the the liquid saturation.

Material	Input parameters	Crit. rad. r_c (nm)	Estimated s_L	Regime
Ionomer	$\theta = 68°$, 7 bar	65-70	0.4-0.5	Liquid-filled
Non-ionic polymer	$\theta = 130°$, 3.5 bar	-	< 0.1	Gas-connected

Table S1: Estimated liquid saturation (of secondary pores) based on supersaturation pressures and contact angles.

In the non-ionic binder-based electrode, the pores appear essentially liquid-free, while for the ionomer-based electrode, around half of the pore volume remains filled with water. At such high liquid saturations, the network of gas-filled pores may become increasingly disconnected. This loss of gas percolation due to partial water filling is represented by a relative gas permeability $k_\mathrm{r,g}(s_\mathrm{L})$

$$k_{r,g}(s_\mathrm{L}) = (1 - s_\mathrm{L})^n \tag{S12}$$

with an exponent n reflecting pore connectivity and wettability effects, generally in the range of $2 < n < 4$ for electrolyser electrodes. This readily suggests that the effective gas permeability in the heavily liquid-filled ionomer-based electrode is reduced almost ten-fold (assuming n=3[S12]).
The *Knudsen number* of the presented hydrogen transport through the pores $K_\mathrm{n} = \frac{\lambda}{r_\mathrm{c}}$ is estimated around 1.3-1.5, with the mean free path of H_2 at 60 °C around 100 nm[S13]; leading to the conclusion that continuum models (Navier-Stokes/Darcy, $K_\mathrm{n} < 0.01$) would exceed their limits of validity.

For the purposes of obtaining a first set of conclusions, a Knudsen description is used here as a limiting case to illustrate the sensitivity of gas transport to liquid saturation; for in-depth derivation of transport at the transition regime around K_n, the reader is referred to e.g. the Bosanquet approximation.[S8,S14] In such Knudsen description, the gas diffusivity becomes[S15]

$$D_{\mathrm{eff,g}}(s_\mathrm{L}) = D_\mathrm{K}\,\frac{\varepsilon}{\tau}\,k_{\mathrm{r,g}}(s_\mathrm{L}), \tag{S13}$$

with the Knudsen gas diffusivity $D_\mathrm{K} = \frac{2}{3}\sqrt{\frac{8RT}{\pi M}}r_\mathrm{c}$, for H_2 at 60 °C $\approx 1.25\,10^3 r_\mathrm{c} \approx 9.4\,10^{-5}$ m^{2}s^{-1} (with molar mass 2 g mol^{-1} for H_2), porosity ϵ and tortuosity τ. In turn, following Fick's law, the gas-phase pressure drop across an electrode of thickness δ^elec carrying a molar hydrogen gas flux out of the electrode $J_{\mathrm{H_2}}^\mathrm{bulk}$ formally becomes

$$\Delta p_\mathrm{g}(s_\mathrm{L}) = \frac{RT\,\delta^\mathrm{elec}}{D_{\mathrm{eff},g}(s_\mathrm{L})}\,J_{\mathrm{H_2}}^\mathrm{bulk} \tag{S14}$$

and therefore ultimately

$$\Delta p_\mathrm{g}(s_\mathrm{L}) \;\propto\; (1-s_\mathrm{L})^{-n} \tag{S15}$$

This equation links the electrode contact angle directly to the supersaturation pressure. Either the pressure drop across the catalyst layer can be obtained from the pore geometries, or, assuming the 7 bar supersaturation and from the derivation above as well as ϵ=0.7, first conclusions can be drawn regarding e.g. the catalyst layer pores. A straight calculation yields an apparent tortuosity of $\tau \approx 10^3$, which has to be considered unrealistically high for catalyst layers; mathematically, as $\Delta p \propto \frac{\tau}{r_\mathrm{eff}}$, very small critical pore radii $\ll 1$ nm would be implied to bring τ into physically meaningful ranges (1$<\tau<$10). Rather, it appears that the measured cathodes comprise a superposition of multiple transport regimes, combining molecular diffusion in the 50-100 nm regime with viscous continuum flow in µm pores:

$$J_{\mathrm{H_2}}^\mathrm{bulk} \propto \frac{D}{RT}\Delta p + \frac{k}{\mu}\Delta p \tag{S16}$$

in a description comprising a dynamic viscosity μ.

In conclusion, under these coarse model assumptions, it is evident how an increased contact angle in the non-ionic binder electrode is linked to lower liquid saturation of the catalyst layer, and in turn, reduced hydrogen crossover.

Addendum 1: Effective diffusion coefficient in swollen membrane.

The permeability of the dry Evonik AEM was estimated around 1.1 ± 0.3 10^{-15} mol m^{-2} s^{-1}Pa^{-1} in a differential pressure setup. From physicochemical models for gas diffusion in alkaline water salt solutions as derived in our earlier report[S1], a solubility of hydrogen gas in 1 M potassium hydroxide solution at 70 °C of $S_{\mathrm{H_2}}^\mathrm{elec}$ of 5.2 10^{-6} mol m^{-3} Pa^{-1} and a diffusion coefficient of $D_{\mathrm{H_2}}^\mathrm{elec}$ of 9.1 10^{-9} m^2 s^{-1} are obtained. In consequence, the permeability of hydrogen gas through the potassium hydroxide is estimated around $P_{\mathrm{H_2}}^\mathrm{elec} = S_{\mathrm{H_2}}^\mathrm{elec} \cdot D_{\mathrm{H_2}}^\mathrm{elec} = 4.7\ 10^{-14}$ mol m^{-2} s^{-1} Pa^{-1}. Therefore, the permeation of hydrogen gas through the liquid phase of the KOH-swollen membrane is estimated to be 50-fold faster than permeation through polymer domains. In consequence, for

the following estimation, we allow the assumption that hydrogen diffusion mainly occurs through the aqueous phase.

The fraction liquid volume ϵ in the Evonik membrane in 1 M KOH at 70 °C was estimated around 0.2 (=20%). Following the commonly applied Bruggeman correlation[S16], the effective diffusion through the swollen membrane $D^{\text{eff}}_{\text{H}_2}$ scales with the volume ratio of the liquid phase ϵ (for the here-described Evonik AEM ≈ 0.2), as well as the diffusion coefficient of hydrogen gas in a bulk electrolyte solution $D^{\text{elec}}_{\text{H}_2}$.

$$D^{\text{eff}}_{\text{H}_2} = \frac{\epsilon_{\text{m}}}{\tau} D^{\text{elec}}_{\text{H}_2} \tag{S17}$$

The tortuosity τ (unitless variable, $\tau \geqslant 1$) describes the '*degree of curvature*' of the liquid channels; e.g. for perfectly linear 'channel-like' structures, τ=1 and $D^{\text{eff}}_{\text{H}_2} = \epsilon_{\text{m}} D^{\text{elec}}_{\text{H}_2}$, and the further τ deviates from unity, the more the hydrogen transport is impeded. Therefore, the physical limit of the effective diffusion coefficient of the swollen membrane (in the ideal approximation of no tortuosity) is $D^{\text{eff}}_{\text{H}_2} = \epsilon_{\text{m}} D^{\text{elec}}_{\text{H}_2}$ = 1.8 10^{-9} m^2 s^{-1}.

Comparing the diffusion coefficients fitted to the experimental model to this theoretical limit, it becomes apparent that the fitted diffusion coefficients $D^{\text{eff}}_{\text{H}_2}$ of 2 10^{-8} m^2 s^{-1} seem to surpass this boundary. In consequence, a secondary fitting of the experimental data is carried out by setting the upper boundary value of $D^{\text{eff}}_{\text{H}_2} = \epsilon_{\text{m}} D^{\text{elec}}_{\text{H}_2}$. Mathematically, higher $p^*_{\text{H}_2}$ would be required to reach

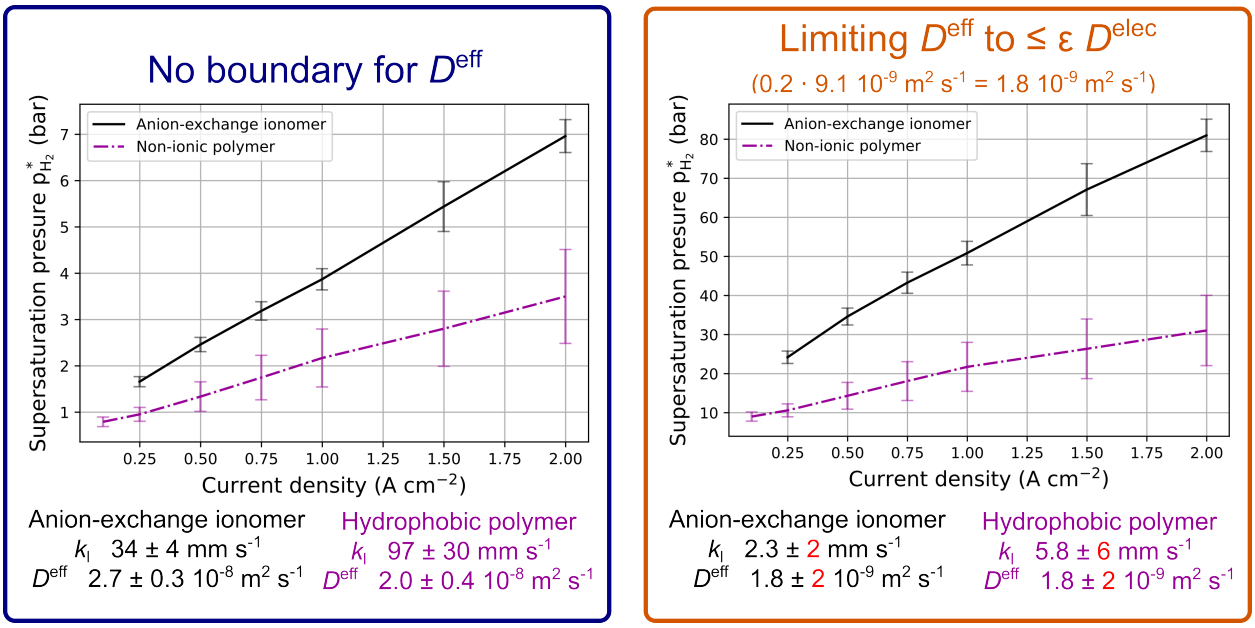

Figure S2: Supersaturation pressures in the cathode catalyst layer when no boundary (left) or $\epsilon_{\text{m}} D^{\text{elec}}_{\text{H}_2}$ (right) is set as boundary condition for $D^{\text{eff}}_{\text{H}_2}$.

the experimentally measured J_{exp} values with lower diffusion coefficients. Indeed, attempting to solve the hydrogen flux model with $\epsilon_{\text{m}} D^{\text{elec}}_{\text{H}_2}$ as upper boundary condition for $D^{\text{eff}}_{\text{H}_2}$ shows that the model converges onto the upper boundary for $D^{\text{eff}}_{\text{H}_2}$, resulting in larger $p^*_{\text{H}_2}$ up to 80 bar at 2 A cm^{-2}

in case of the electrode based on the anion-exchange ionomer (Fig. S2). However, the uncertainties of k_l and $D^\mathrm{eff}_{\mathrm{H_2}}$ are as large as their absolute values, rendering this parameter set a rather poor description of the underlying hydrogen fluxes.
In conclusion, the initially-presented description provides a sufficient model of how the utilisation of a hydrophobic hydrocarbon electrode polymer affords a faster gas transport velocity out of the cathode electrode. Towards a thorough theoretical model, a more sophisticated description is required to match physical properties and fluxes, allowing for e.g. 1) variability of the cathode transport velocity k_l with the current density and 2) variability of $D^\mathrm{eff}_{\mathrm{H_2}}$ at different locations of the membrane (with different local $c_{\mathrm{H_2}}$), which for now lies beyond the scope of this report.

Addendum 2: Formal description of transport processes.
In the description above, the transport of hydrogen out of the cathode due to a concentration gradient towards the bulk solution was described with a transport velocity k_l as $J^\mathrm{bulk}_{\mathrm{H_2}} = k_l \left(c^*_{\mathrm{H_2}} - c^c_{\mathrm{H_2}}\right)$, while the (diffusive) transport through the membrane due to a concentration gradient towards the anode was described with by means of an effective diffusion coefficient $J^\mathrm{diff}_{\mathrm{H_2}}$ as $J^\mathrm{diff}_{\mathrm{H_2}} = \frac{D^\mathrm{eff}_{\mathrm{H_2}}}{\delta_\mathrm{m}} \left(c^*_{\mathrm{H_2}} - c^\mathrm{a}_{\mathrm{H_2}}\right)$. While this is likely the most-suitable physical description, it renders the implication of the two transport processes somewhat unintuitive to compare. For comparison purposes, one may therefore introduce a pseudo-velocity k_l^membrane as $J^\mathrm{diff}_{\mathrm{H_2}} = k_l^\mathrm{membrane} \left(c^*_{\mathrm{H_2}} - c^\mathrm{a}_{\mathrm{H_2}}\right)$, or $k_l^\mathrm{membrane} = \frac{D^\mathrm{eff}_{\mathrm{H_2}}}{\delta_\mathrm{m}}$. A k_l^membrane around 2 10^{-4} m s^{-1} is obtained, compared to 3 10^{-2} m s^{-1} for the hydrogen transport out of the cathode (Tab. S2). This shows that the hydrogen transport out of the catalyst layer is more than 100-fold faster than crossover transport, consistent with hydrogen crossover values of few percent.

Table S2: Transport velocities of hydrogen out of the cathode catalyst layer and through the anion-exchange membrane (all in m s^1).

	Anion-exchange ionomer	Hydrophobic polymer
$k_\mathrm{l}^\mathrm{electrode}$	$3.4 \pm 0.4\ 10^{-2}$	$9.8 \pm 0.4\ 10^{-2}$
$k_\mathrm{l}^\mathrm{membrane}$	$2.4 \pm 0.4\ 10^{-4}$	$2.0 \pm 0.4\ 10^{-4}$

Durability testing.

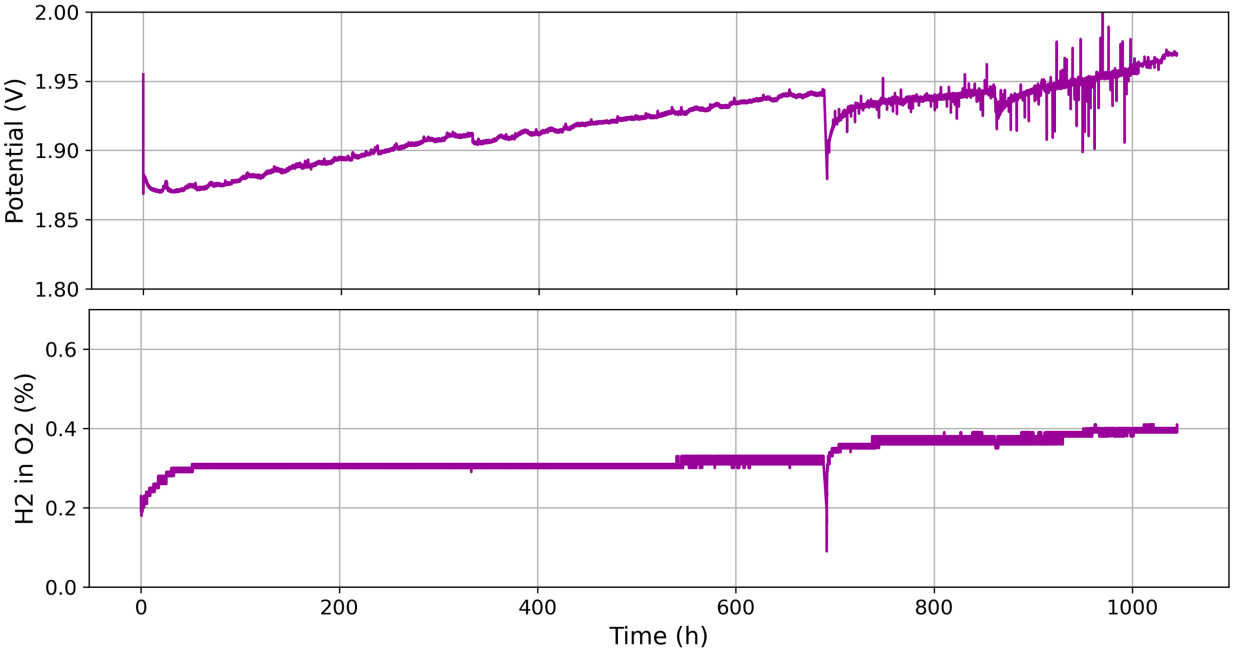

Figure S3: Durability test of direct-membrane-coated cathode based on the non-ionic binder polymer at 1.5 A cm^{-2}, 60 °C, 1 M KOH (dual feed, in combination with a Siemens Energy carbon felt contacting the cathode). At 680 operating hours, an electrolyte pump outage temporarily interrupted the test.

Dry-cathode operation.

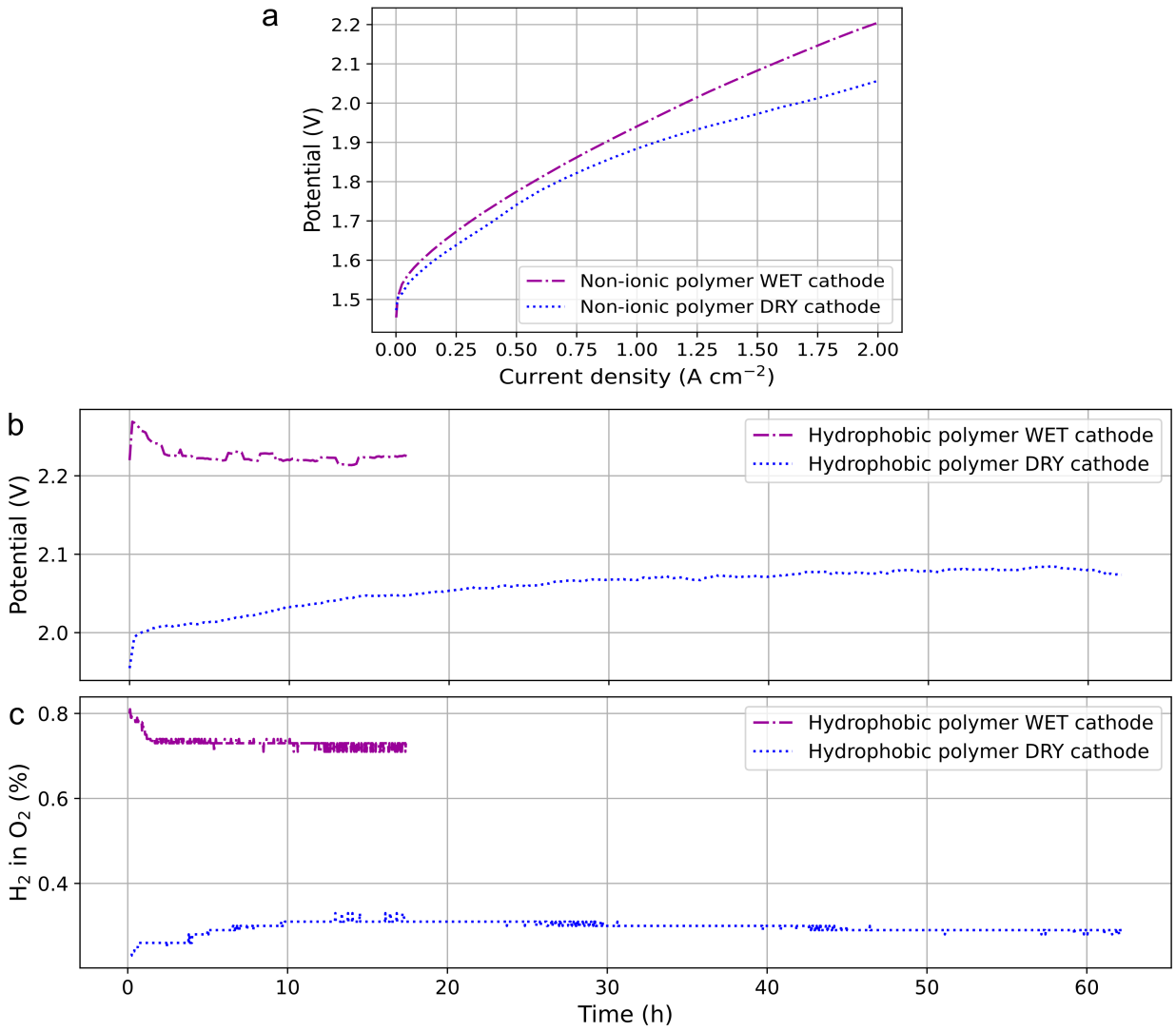

Figure S4: Dry-cathode operation of cathodes based on non-ionic cathode binder polymer in a constant-current hold at 1.5A cm^{-2}.

Time-series data of hydrogen crossover during staircase profile.

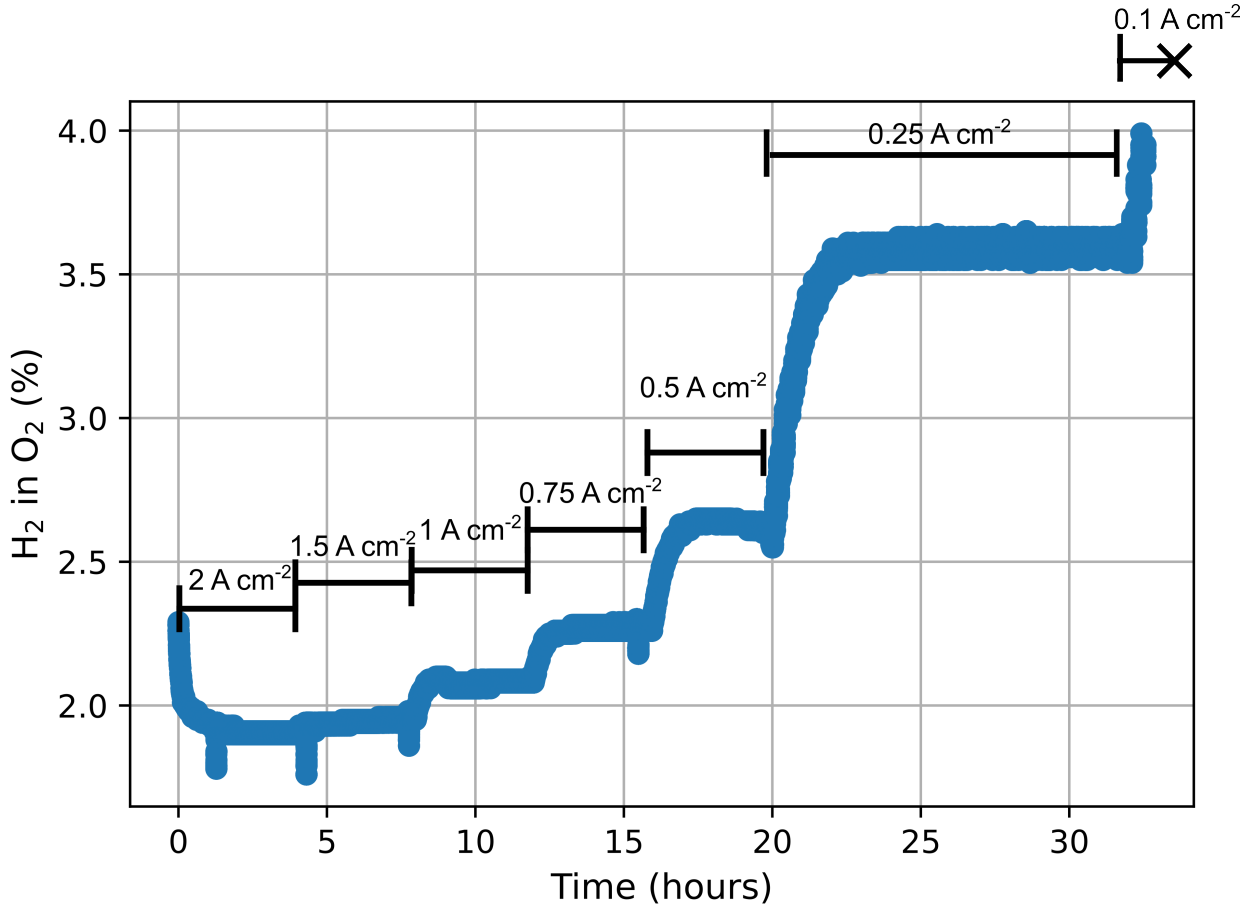

Figure S5: Hydrogen crossover during staircase profile operation of an electrode based on the anion-exchange ionomer. At 0.1 A cm^{-2}, the H_2-in-O_2-value hit 4% and a safety shutoff of the experiment was automatically triggered.

Determination of the drag coefficient.

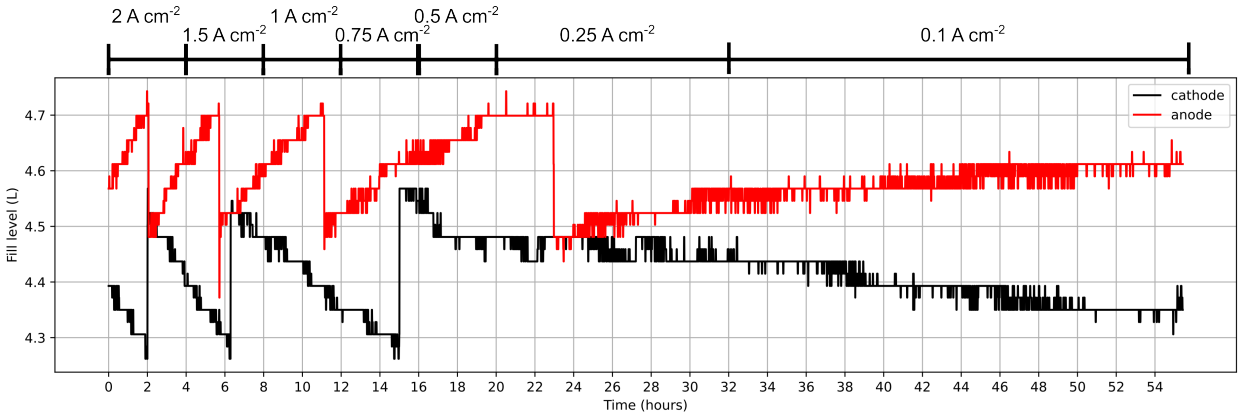

Figure S6: Anode and cathode fill levels during staircase profile.

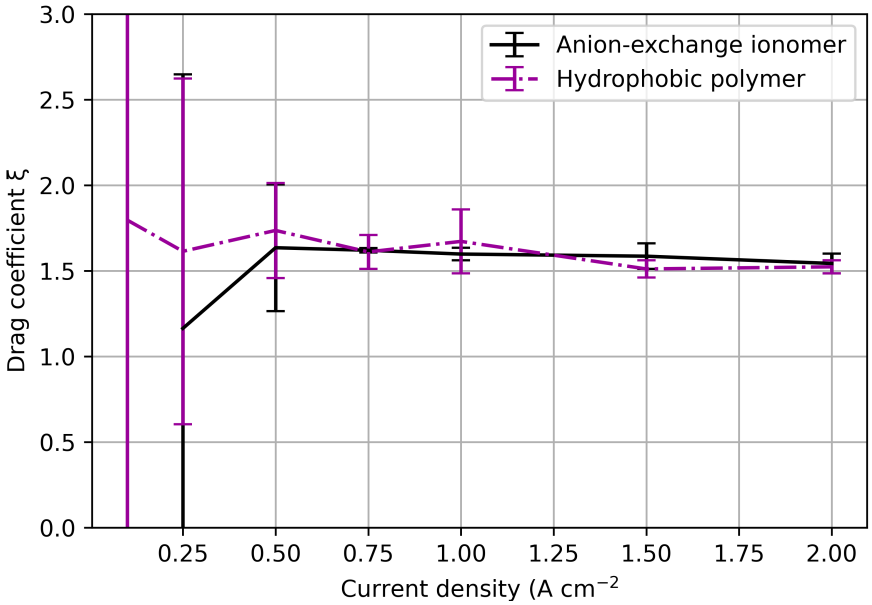

Figure S7: Drag coefficient of Evonik membrane.

Expected hydrogen crossover dependence on membrane thickness.

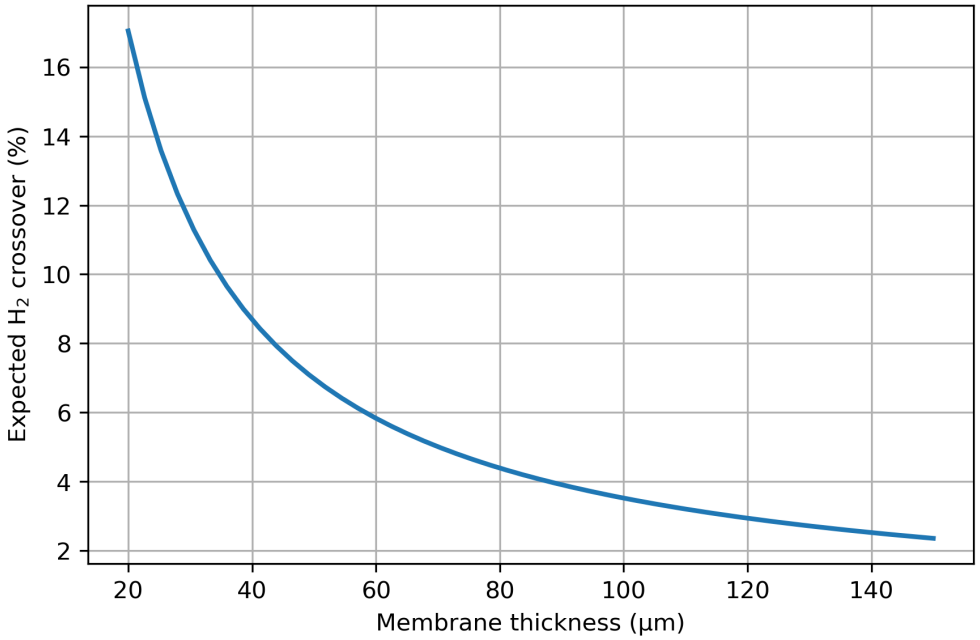

Figure S8: Expected hydrogen crossover dependence on wet membrane thickness at 0.25 A cm^{-2}. All model parameters were adapted from the ionomer-based experiments (e.g. giving 3.5% at 98 μm effective wet thickness membrane). It is evident that to bring the hydrogen crossover down to $< 2\%$, membrane thicknesses of $>$150 μm would be required.

Zeta-Potential.

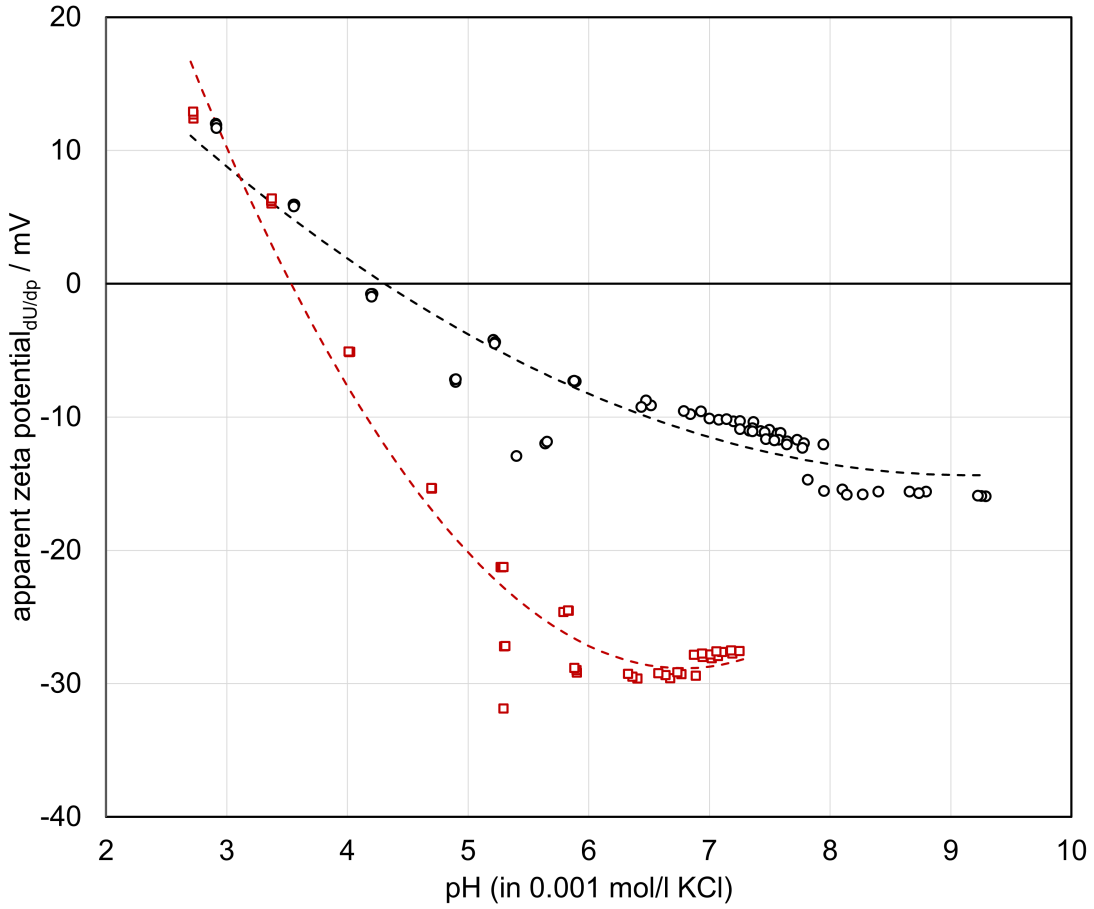

Figure S9: pH-dependence of the apparent zeta potential for the anion-exchange ionomer (black circles) and the hydrophobic polymer (red squares) binder paste.

Physisorption.

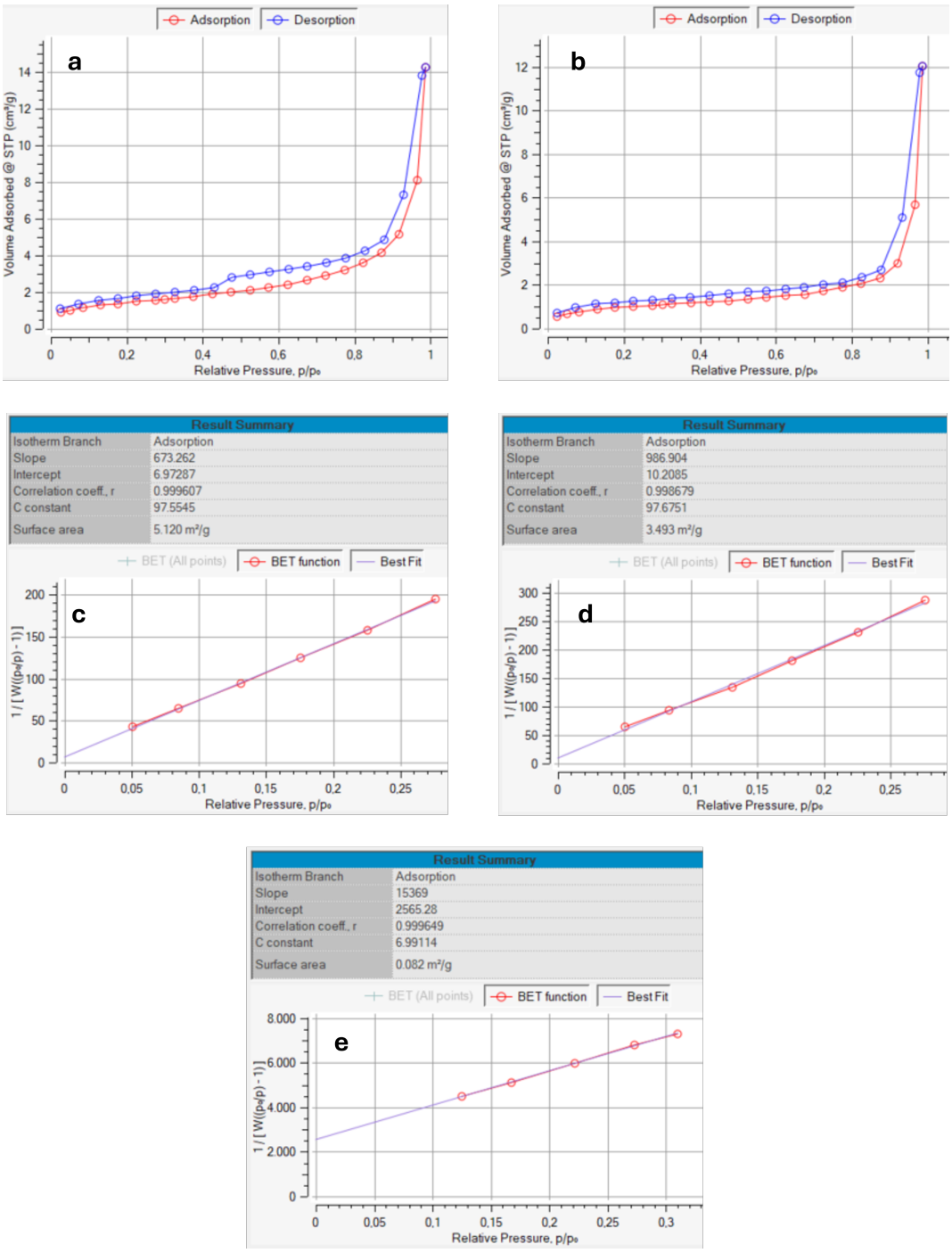

Figure S10: Exemplary nitrogen physisorption isotherm of direct-membrane-coated cathodes based on **a.** the anion-exchange ionomer and **b.** the non-ionic polymer binder paste. Corresponding BET plots for the direct-membrane-coated cathodes based on the **c.** anion-exchange ionomer and **d.** the non-ionic polymer binder paste. **e.** BET plot for the bare membrane (using Kr as adsorptive).

Porometry.

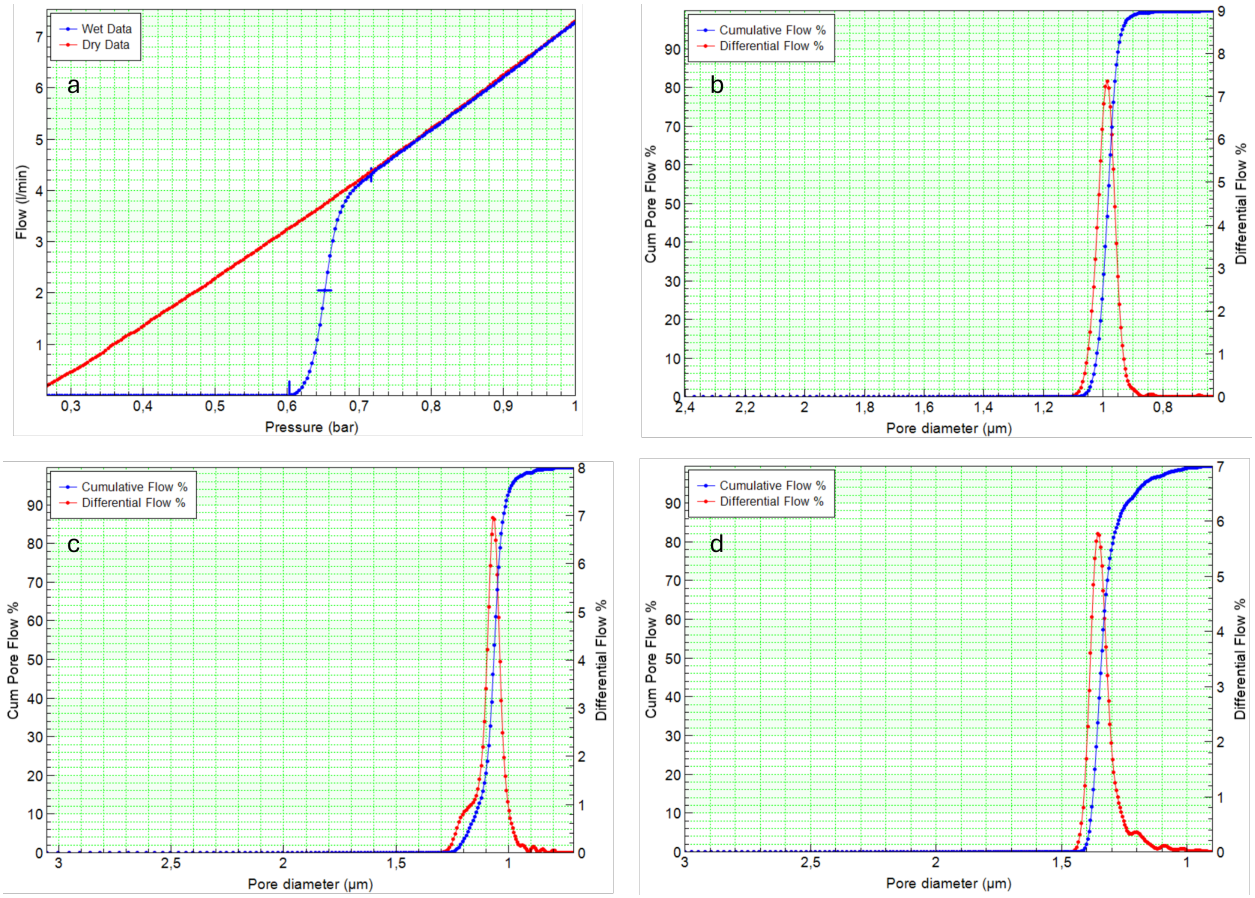

Figure S11: **a.** Exemplary capillary flow porometry measurement of the anion-exchange ionomer binder paste and the resulting through pore size distribution of the anion-exchange ionomer (**b.**), the non-ionic polymer binder paste (**c.**), and the blank carbon felt (**d.**).

Supporting references

[S1] Klinger A, Strobl O, Michaels H, Kress M, Martic N, Maltenberger A, et al. Transport of Hydrogen Through Anion Exchange Membranes in Water Electrolysis. Advanced Materials Interfaces. 2025;12(5).

[S2] Ge S, Yi B, Ming P. Experimental Determination of Electro-Osmotic Drag Coefficient in Nafion Membrane for Fuel Cells. Journal of The Electrochemical Society. 2006;153(8):A1443.

[S3] Eikerling M. Water Management in Cathode Catalyst Layers of PEM Fuel Cells. Journal of The Electrochemical Society. 2006;153(3):E58.

[S4] Weber AZ, Newman J. Transport in polymer-electrolyte membranes: II. Mathematical model. Journal of The Electrochemical Society. 2004;151:A311-25.

[S5] de Gennes PG, Brochard-Wyart F, Quéré D. Capillarity and Wetting Phenomena. Springer; 2004.

[S6] Evans R, Marconi UMB, Tarazona P. Capillary condensation and adsorption in cylindrical and slit-like pores. Journal of Chemical Physics. 1986;84:2376-89.

[S7] Dunlap PM, Faris SRAM. Surface Tension of Aqueous Solutions of Potassium Hydroxide. Nature. 1962;196(4861):1312-3.

[S8] Bierling M, McLaughlin D, Hutzler A, Wu M, Hoffmeister D, Chalupczok D, et al. Laying the Foundation for Digital Material Design of Porous Transport Electrodes for PEM Water Electrolysis With Multiscale Tomography. Small. 2026;22(22):e13029.

[S9] Soboleva T, Zhao X, Malek K, Xie Z, Navessin T, Holdcroft S. On the micro-, meso-, and macroporous structures of polymer electrolyte membrane fuel cell catalyst layers. ACS applied materials & interfaces. 2010;2(2):375-84.

[S10] Olbrich W, Kadyk T, Sauter U, Eikerling M. Review—Wetting Phenomena in Catalyst Layers of PEM Fuel Cells: Novel Approaches for Modeling and Materials Research. Journal of The Electrochemical Society. 2022;169(5):054521.

[S11] Girod R, Lazaridis T, Gasteiger HA, Tileli V. Three-dimensional nanoimaging of fuel cell catalyst layers. Nature catalysis. 2023;6(5):383-91.

[S12] Meng H. Numerical studies of liquid water behaviors in PEM fuel cell cathode considering transport across different porous layers. International Journal of Hydrogen Energy. 2010;35(11):5569-79.

[S13] Reid RC, Prausnitz JM, Poling BE. The Properties of Gases and Liquids. 4th ed. New York: McGraw–Hill; 1987.

[S14] Pollard WG, Present RD. On Gaseous Self-Diffusion in Long Capillary Tubes. Physical Review. 1948;73(7):762-74.

[S15] Mason EA, Malinauskas AP. Gas Transport in Porous Media: The Dusty-Gas Model. Elsevier; 1983.

[S16] Tjaden B, Cooper SJ, Brett DJL, Kramer D, Shearing PR. On the origin and application of the Bruggeman correlation for analysing transport phenomena in electrochemical systems. Current Opinion in Chemical Engineering. 2016;12:44-51.